New Cosmological Data and the Values of the Fundamental Parameters
IAU Symposium, Vol. 201, 2005
Anthony Lasenby and Althea Wilkinson, eds.

DASI: The Degree Angular Scale Interferometer

E. M. Leitch, J. E. Carlstrom, G. Davidson, M. Dragovan, N. W. Halverson, W. L. Holzapfel, S. Laroque, J. Kovac, C. Pryke, E. Schartman, M. J. Yamasaki

University of Chicago, 5640 S. Ellis Avenue, Chicago, IL 60637, USA

Abstract. We describe the design and current status of the Degree Angular Scale Interferometer (DASI), a compact cm-wave interferometer operating at the Amundsen-Scott South Pole research station. With 20-cm diameter primary antenna elements operating over the frequency range 26 – 36 GHz, DASI is optimized to measure the power spectrum of the cosmic microwave background radiation (CMBR) over the multipole range 140 – 920, (corresponding to scales of $25' - 2.^\circ 6$), as well as make high-sensitivity maps of the microwave sky. The telescope was built at the University of Chicago and deployed at the South Pole during the 1999–2000 austral summer.

1. Introduction

The DASI telescope is the outgrowth of a collaboration between the University of Chicago and the California Institute of Technology; the Cosmic Background Imager (CBI), the companion project to DASI, is described elsewhere in this volume. DASI is designed to provide sensitivity to the CMBR at intermediate angular scales, while the CBI extends this coverage to very small-scales. The maximum baseline separation, which sets the smallest angular scale DASI can resolve, is 120 cm, while the minimum baseline length is 25 cm, chosen to complement experiments probing the first acoustic peak. Together, these two experiments will provide continuous coverage of the CMBR power spectrum from $l = 140$ to $l = 3500$. The DASI bandpass is correlated in 10 1-GHz channels, providing spectral leverage for discrimination of foregrounds, as well as allowing frequency synthesis mapping in the image plane. An extremely sensitive imaging instrument, DASI can achieve 10 μK rms at $20'$ resolution over its $3.^\circ 4$ field of view in 24 hours.

2. Instrument Design

2.1. Telescope Mount

The telescope is situated atop the inner of two concentric towers attached to the Martin A. Pomerantz Observatory (MAPO) at the South Pole station (see Figure 1); the inner tower is mechanically isolated from the outer tower, so that no vibration can be transmitted from the building to the telescope. A room beneath the telescope, vibrationally isolated from the telescope, houses helium compressors, drive amplifiers, and an air handling unit for managing waste heat

Figure 1. The DASI telescope (left) being lifted to the 35-ft tower attached to the MAPO building at the Amundsen-Scott South Pole Station 3 December 1999 and (right) operating at sunset March 2000.

from the telescope and helium compressors. The interior of the telescope opens directly onto the compressor room, providing access to drive systems, receivers and electronics even in mid-winter, when the darkness and extreme cold (as low as $-80°$ C ambient) severely restrict outside activity. An insulated fabric bellows allows motion in the elevation axis while keeping the interior of the telescope and drive assemblies at room temperature.

The telescope consists of an altitude-azimuth mount, employing a counterbalanced gear and pinion elevation drive, yielding excellent tracking and pointing stability. Heavy box steel-plate construction lends the mount extreme rigidity and immunity to flexure. The interferometer has 13 primary antenna elements, arranged in a three-fold symmetric pattern on a rigid faceplate, which attaches to the elevation cradle.

The faceplate can also be rotated about its axis; in combination with the three-fold symmetry, this feature provides important diagnostic capabilities, for instance permitting discrimination of spurious signals due to cross-talk between the antenna elements, a concern with any compact array in which the elements are nearly touching. Since the antenna pattern repeats with every $120°$ of rotation, any signal in the far field will be unchanged by the rotation, while any signal due to cross-talk will rotate with the faceplate. For purposes of imaging, the rotation also allows dense sampling of the $u - v$ plane.

In addition, the rigid faceplate greatly simplifies the design of an interferometer. Unlike conventional tracking arrays, projected baseline lengths for a co-planar array are independent of the pointing center, and IF tracking delays are not required.

https://doi.org/10.1017/S0074180900216070 Published online by Cambridge University Press

2.2. Primary Antenna Elements

Each of DASI's 13 primary antenna elements consists of a 20-cm diameter, wide flare-angle corrugated horn; to make the array maximally compact, the receiver dewars were designed to fit entirely within the footprint of the horns. Unlike mini-Cassegrain elements, horns provide unobstructed apertures, with correspondingly lower sidelobe response and better cross-talk characteristics. To further reduce cross-talk from correlated amplifier noise, the receivers are equipped with front-end isolators, and each antenna element is in turn surrounded by a corrugated shroud.

Each element is preceded by a high density Polyethylene lens, permitting a very compact horn design, while at the same time flattening the aperture distribution, resulting in a high aperture efficiency — 84%, compared to 69% for an unlensed horn. At polar temperatures, the lens contributes no more than 2.5 K to the system temperature.

The measured beam pattern, which determines the field of view of the interferometer, has a FWHM of $3\overset{\circ}{.}4$, with first sidelobes below -20 dB, in excellent agreement with the predicted pattern.

2.3. Signal Chain

Each horn feeds a cryogenically cooled 4-stage InP HEMT amplifier operating between $26 - 36$ GHz. The amplifiers were constructed at the University of Chicago, after a design developed at NRAO (Pospiezalski 1993, Pospiezalski et al. 1994). Receiver temperatures range between $18 - 25$ K at the center of the band, including the warm lens, feed horn and throat, and cold isolator and polarizer. Including CMBR and atmosphere, we achieve typical system temperatures of 25 K, for an rms sensitivity of approximately 0.8 mK $s^{1/2}$ in a 1 GHz band on a single baseline.

The RF signal from each antenna is mixed down to $2 - 12$ GHz IF using a local oscillator tuned to 38 GHz. The IF signal is then split into 10 1-GHz bands, each of which is further mixed down to $1 - 2$ GHz. The 13 signals at each frequency are fed to one of 10 identical analog correlators, where the 78 complex multiplications are formed, digitized and integrated for 0.84 s in a digital accumulator. A phase switch is applied to each LO in a Walsh sequence on a 25.6 μs clock interval and is demodulated by the accumulators, to remove any offsets or slowly varying pickup. A second level of Walsh switching is performed in software with a switching period equal to the readout interval. The multiplier gains and quadrature errors are periodically calibrated by injection of a correlated broadband noise source at the input to each receiver.

Each analog correlator is integrated onto a single full-depth VME card, and the entire 10-GHz correlator fits into a crate approximately 75 cm on a side. Filtering and downconversion of the IF signal is accomplished in a similar crate, and both rotate with the antennas on the underside of the telescope faceplate. The short fixed distance to the downconverter and correlator provides tremendous phase stability, with observed instrumental phase drifts of less than 10° over a period of weeks.

https://doi.org/10.1017/S0074180900216070 Published online by Cambridge University Press

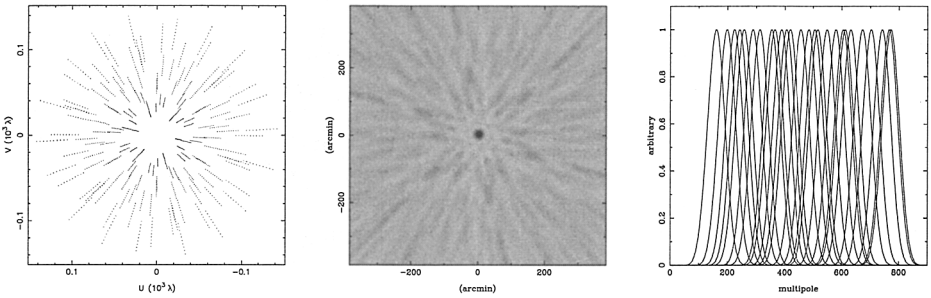

Figure 2. Fourier-plane and imaging characteristics of the DASI instrument. The instantaneous $u-v$ coverage of the interferometer (left), and the resulting synthesized beam (center) for natural weighting, with approximately $20'$ FWHM. (right) The corresponding l-space coverage at 30 GHz. Note that the three-fold symmetry results in only 26 independent baseline lengths at each frequency.

2.4. Interferometer Characteristics

The left panels of Figure 2 show the DASI instantaneous $u-v$ coverage and the corresponding synthesized beam in the image plane. Besides yielding spectral information, the 10 1-GHz channels allow frequency synthesis mapping, since for any given baseline, the corresponding $u-v$ radius varies by 30% over the 10 GHz band, hence the radial pattern in the $u-v$ coverage. The effective snapshot resolution when all 10 bands are combined is approximately $20'$, as shown in the central panel.

Figure 2 also shows the effective sensitivity of the instrument in l-space. The right panel is an azimuthally collapsed composite of the l-space window functions for all independent baselines at a single frequency. Exact antenna spacings on the faceplate were numerically optimized to yield uniform $u-v$ coverage over the angular range accessible to DASI. Note that the finite aperture introduces correlations between baselines at neighboring $u-v$ points, particularly between visibilities of the same baseline at neighboring frequencies.

With the three-fold redundancy, the pattern of $u-v$ coverage repeats with each $60°$ of rotation. Although the antenna locations repeat only every $120°$, the same Fourier components of the sky are measured under reflection of the array, since the sky is real and its transform Hermitian.

3. Site Characterization

Extreme desert conditions at the South Pole make it an excellent site for radio astronomy, apart from the obvious advantage of six months without sun. Due to the flattening of the atmosphere at the poles (the tropopause occurs at approximately 7 km above the South Pole, compared to 11 km at more equatorial latitudes) and the physical elevation of 2.8 km, the site is above much of the atmospheric water vapor. Moreover, with an average year-round temperature of $-47°$ C, the residual atmosphere is quite cold.

https://doi.org/10.1017/S0074180900216070 Published online by Cambridge University Press

From load calibrations performed during the austral summer, we determined the mean zenith opacity over the DASI bandpass to be $\tau \sim 0.02$. The opacity shows little day-to-day variation, as determined from skydips performed twice daily throughout the year. At typical ambient temperatures during the winter ($-60°$ C), these results suggest that over much of the DASI bandpass, the atmosphere contributes little more to our system temperature than the CMBR.

The Python experiment, which operated at the South Pole during the 1996-1997 austral summer, found that the atmosphere could rarely be seen in the data; the experiment was noise limited 75% of the time (Lay & Halverson 2000). DASI data suggest that during the austral winter, the efficiency is closer to 90%.

4. Calibration

The relative scarcity of sources whose absolute fluxes are known at these frequencies makes calibration of any microwave experiment a challenging proposition, as does the generic steepness of most radio source spectra. Additionally, of the sources which are well studied, few are accessible from the South Pole (and planets, when they are visible at all, never rise more than $23\overset{\circ}{.}5$ above the horizon). Moreover, with DASI's 20-cm apertures, beam dilution makes it inherently difficult to detect all but the brightest point sources. The gain of the telescope is approximately 10 μK/Jy, so that for a single baseline, to achieve a signal/noise ~ 1 on a 1 Jy source requires about 3 hours of observation.

Accordingly, the absolute calibration of DASI was initially based on observations of Eta Carinae, a well-known Galactic HII complex. While point-like sources are more convenient, a source of arbitrary complexity can in principle be used as a flux calibrator, provided its flux can be determined for each baseline. DASI's simple horn design allows an accurate calculation of the theoretical aperture efficiency, and fluxes for the source are based on absolute load calibrations transferred to Eta Carinae in February 2000.

Eta Carinae's free-free spectrum makes it a good high frequency calibrator; the source is bright enough that its flux can be measured to a few percent on most baselines in approximately 15 minutes. As can be seen from Figure 3, however, the source is dominated by a bright central region, with much weaker flux on smaller scales, necessitating significantly longer integrations on the longest baselines to achieve uniform accuracy. These considerations have led us to transfer the Eta Carinae calibration to PKS B0857-473, a more compact Galactic HII region also observed by the BOOMERANG experiment (de Bernardis et al. 2000). Although its integrated flux is lower than that of Eta Carinae, as can be seen from Figure 3, the source is readily detectable, and uniformly bright even at our longest baselines.

Observations of the phase stability while tracking PKS B0857-47 demonstrate that it is sufficiently point-like (or at least radially symmetric), and that the background is sufficiently uniform, that the source is also suitable as a phase calibrator.

Recently, simultaneous DASI and CBI observations of a bright point source visible both from the South Pole and Cerro Chajnantor in Chile, have established a common flux scale between these experiments, effectively linking the DASI calibration to the brightness temperature of Jupiter.

https://doi.org/10.1017/S0074180900216070 Published online by Cambridge University Press

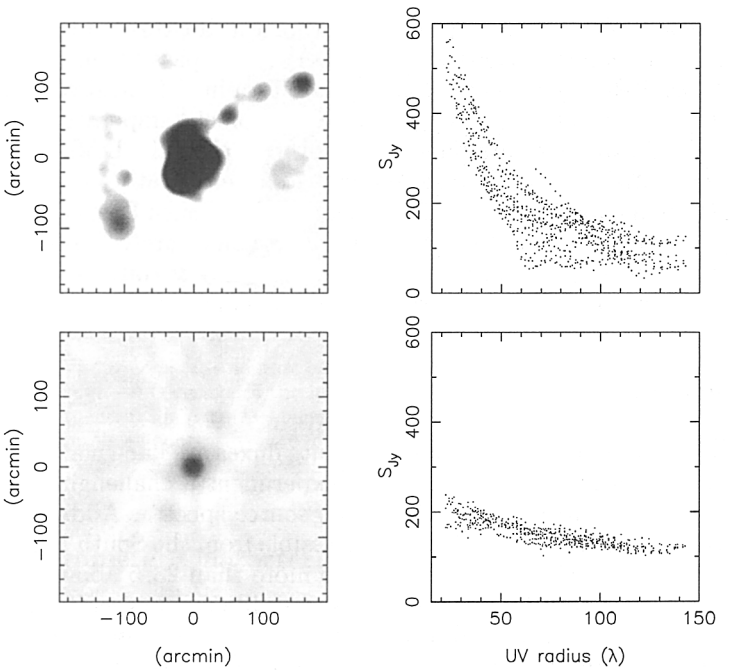

Figure 3. DASI images of calibration sources. Eta Carinae is shown at top left, with the central complex suppressed so that the substructure can be seen. The sharp fall-off of the flux with $u-v$ radius (top right) degrades the accuracy of long baseline calibrations. The source PKS B0857-473 (bottom left) is much more compact, and is correspondingly brighter than Eta Carinae for baseline lengths $> 80\lambda$.

5. Observations

As with any CMBR experiment, DASI target fields are selected to avoid obvious foreground contaminants. Fortunately, the South Pole provides access to a region of sky with some of the lowest dust column densities, as inferred from the IRAS 100-micron map of the southern sky. Although thermal emission from dust is not expected to be significant at these frequencies, recent observations suggest that non-thermal emission associated with the dust may contaminate small-scale anisotropy measurements at a much higher level (Leitch et al. 1997).

Little is known about the distribution of point sources at these frequencies, and without a dedicated program of followup with a high-gain (K/Jy) instrument, the best that can be done is to avoid known sources from low-frequency surveys. From the DASI data alone, we can identify and remove point sources to approximately 0.25 Jy, and generous assistance by the ATCA facility has provided us with additional observations of contaminating sources. The contribution from sources below the DASI detection threshold will require a statistical correction to the measured power spectrum at our highest-l bins, but we expect this to be quite small.

https://doi.org/10.1017/S0074180900216070 Published online by Cambridge University Press

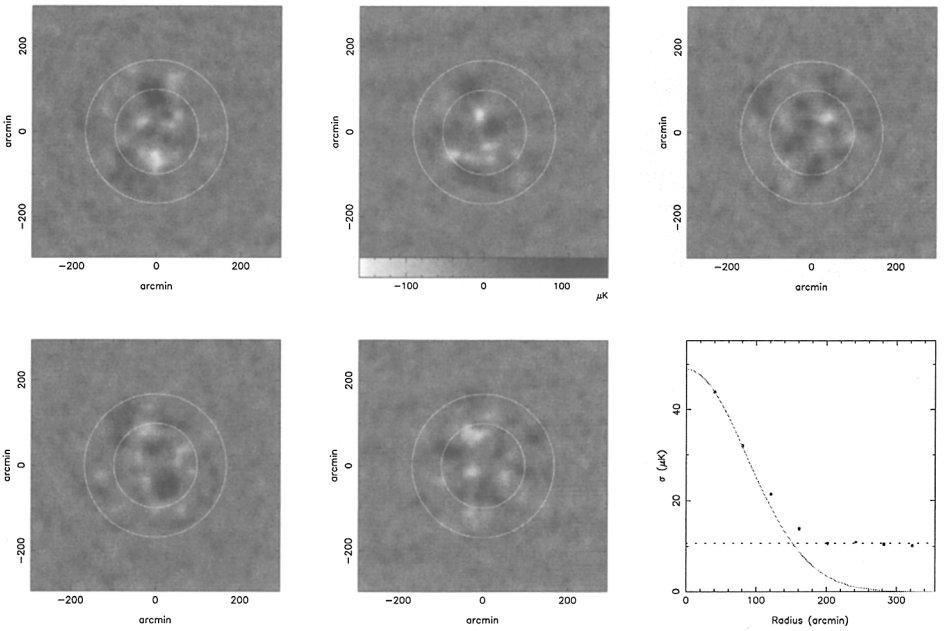

Figure 4. Images of five DASI CMB fields. The two concentric circles represent the −3 dB and −10 dB taper of the beam, respectively. The lower right panel shows the rms pixel values for field 5 (lower middle panel) as a function of radius (black points), the primary beam taper normalized to the first rms pixel value (solid line), and the theoretical rms image noise, determined from the scatter in 8-s visibility data (dashed line). The rms noise tapers with the primary beam sensitivity until it becomes dominated by the instrument noise at the edges of the plots, indicating the origin of the signal is on the sky. The signal level is consistent with that expected from the CMB.

Astronomical foregrounds aside, the presence of ground contamination at a level much greater than the expected cosmological signal places by far the most stringent constraint on our observing strategy. DASI was intended to operate with a ground shield; this could not however be installed until the 2000-2001 austral summer, and was not in place while the data presented here were collected. The signature of the ground is ubiquitous even in the raw visibility data, and is strongly dependent on baseline length, falling sharply with increasing $u - v$ radius.

Accordingly, instead of tracking single fields over the full azimuth range, we observe sets of eight fields, each field in the set spaced by one hour of right ascension. Fields are successively tracked over two narrow azimuth ranges, selected to avoid lines of sight which intersect with station buildings. In this way, during a 24-hour period, we obtain two hours of data on each of eight fields, with the remainder of the time spent on calibration. The number of fields reflects a compromise between our ability to constrain the ground, observing time on each field, and sample variance on the CMBR signal.

https://doi.org/10.1017/S0074180900216070 Published online by Cambridge University Press

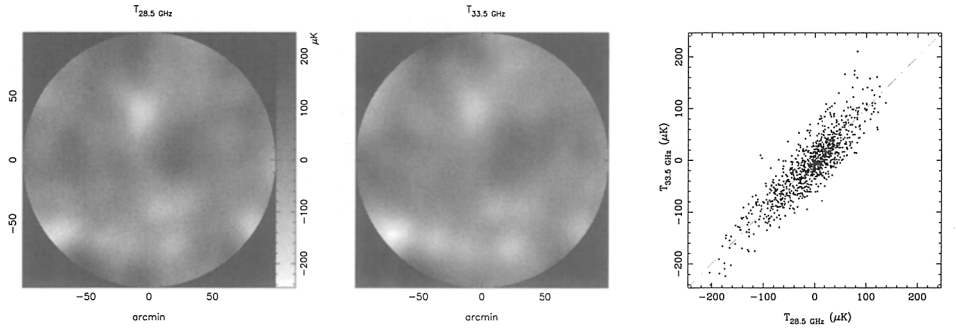

Figure 5. DASI image of a single CMBR field corrected for the primary beam, imaged in two different frequency ranges, 26–31 GHz (left panel) and 31–36 GHz (center panel). The right panel shows the correlations in pixel values between the two images. The images are consistent with one another, indicating the imaged signal is thermal, as expected from the CMBR.

5.1. Effectiveness of Ground Subtraction

Of principal concern is whether and on what timescales the ground signal is repeatable; if it is stable over eight hours, the common signal can be removed from the eight fields at only a small cost in signal/noise on the residual CMBR component. Fortunately, repeated observations demonstrate that the ground signal is stable over several days, and this subtraction scheme has proven successful.

A selection of five such fields is shown in Figure 4, after ground subtraction. In the presence of residual near-field contamination of the visibilities (say, by the ground), these maps would be dominated by large-scale noise across the map. On the contrary, real structure in the far-field will appear enveloped by the primary beam, as can plainly be seen in these images. As the final panel demonstrates, the enveloping of the signal is well matched to the measured beam profile, approaching the theoretical noise floor far from the center of the map.

More quantitative analysis of the distribution of ground-subtracted visibilities confirms this qualitative impression, and shows no evidence for residual ground contamination for $u - v$ radii $> 50\lambda$, and little residual signal even for the shortest baselines.

5.2. Frequency Comparison of Fields

An obvious question which remains is whether the structure in the maps is thermal. For an interferometer, this proves non-trivial to address in the image plane, since the $u - v$ sampling scales with frequency. A simple division of the bandpass into halves, for instance, probes not only different frequencies, but different angular scales as well.

In the maps in Figure 5 we attempt to minimize this complication by imposing a $u-v$ cutoff to equalize the sampling at each frequency, and by deconvolving the resulting sampling function from each map. The primary beam envelope also scales with frequency, and each map has been corrected by the appropriate ta-

https://doi.org/10.1017/S0074180900216070 Published online by Cambridge University Press

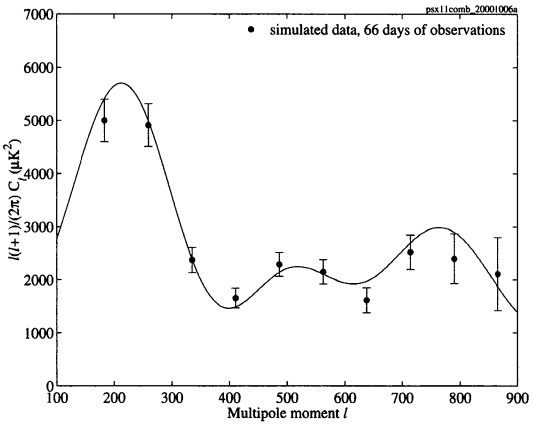

Figure 6. Expected errors on the measured DASI power spectrum, where visibilities have been combined into 10 bins. Points are the power spectrum recovered from a set of 24 simulated CMBR fields, drawn from the power spectrum given by the solid line. No point sources were included in these simulations.

per, so that these represent our best estimate of the actual sky structure at each frequency. A scatter plot of the pixels in this field demonstrates that the maps are consistent with a thermal spectrum.

6. Conclusions

As of sunrise 2000, we have obtained more than 1000 hours of usable data on three sets of eight fields, or over 42 hours per field. DASI images of these fields are shown in Figure 7, with rms noise in each field less than 10 μK (note, however, that these maps have been corrected for the primary beam, so that the signal/noise decreases by a factor of two at the edge).

Figure 6 shows the estimated errors on power spectrum measurements given the data collected so far. Note that this is *not* a power spectrum measured by DASI, but a power spectrum recovered from realistic simulations of the CMBR, with sky coverage and noise appropriate for the data in hand. Errors on these estimates reflect actual data editing and scatter, baseline correlations due to the overlap of antenna apertures in the $u - v$ plane, and correlations introduced by the ground subtraction.

References

de Bernardis, P. et al. 2000, Nature, 404, 955

Lay, O. P. & Halverson, N. W. 2000, ApJ, 543

Leitch, E. M., Readhead, A. C. S., Pearson, T. J. & Myers, S. T. 1997, ApJ486, L23

Pospieszalski, M. W. 1993, in Proc. of 23rd European Microwave Conf. (Madrid), 73

Pospieszalski, M. W., Nguyen, L. D., Lui, M., Lui, T., Thompson, M. A. & Delaney, M. J. 1994, in Proc. 1994 IEEE MTT-S Int. Microwave Symp. (San Diego), 1345

https://doi.org/10.1017/S0074180900216070 Published online by Cambridge University Press

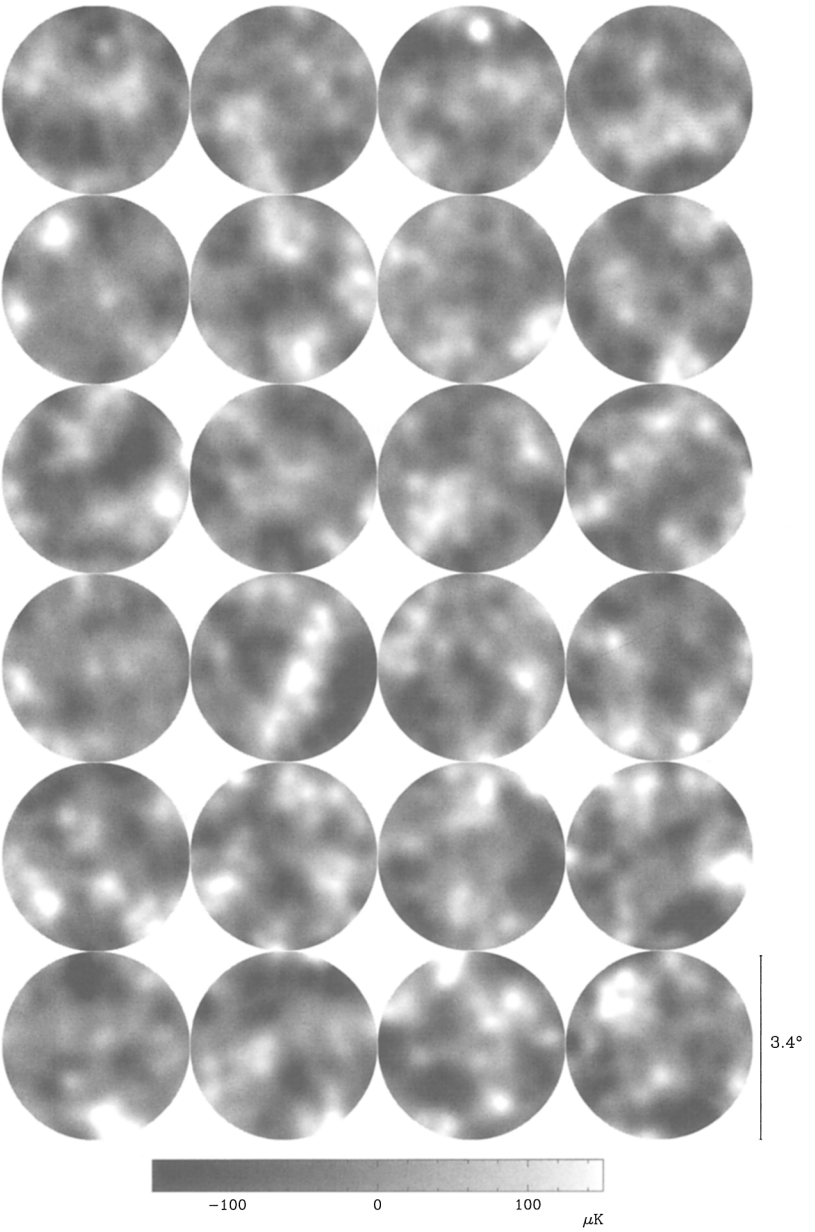

Figure 7. DASI images of 24 CMBR fields, where maps have been corrected for the primary beam taper. Each circle represents the 3.°4 FWHM of the primary beam.

https://doi.org/10.1017/S0074180900216070 Published online by Cambridge University Press